



Declassified by authority of NASA  
Classification Change Notices No. 167  
Dated \*\* 1/15/69

*NEOK*

NACA RM L55L16



# RESEARCH MEMORANDUM

DECLASSIFIED- AUTHORITY MEMO U.S.  
4508  
RICE TO SHAUKLAS DATED 11/21/68

SOME EFFECTS OF ROLL RATE ON THE LONGITUDINAL STABILITY  
CHARACTERISTICS OF A CRUCIFORM MISSILE CONFIGURATION

AS DETERMINED FROM FLIGHT TEST FOR A  
MACH NUMBER RANGE OF 1.1 TO 1.8

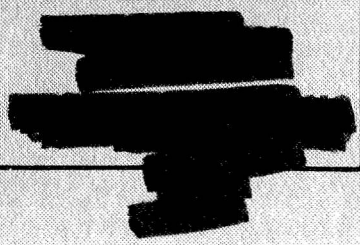
By Reginald R. Lundstrom and Hal T. Baber, Jr.

Langley Aeronautical Laboratory  
Langley Field, Va.



NATIONAL ADVISORY COMMITTEE  
FOR AERONAUTICS

WASHINGTON  
June 19, 1956



N69-71419

(AUTHOR)	<i>Lundstrom</i>	(CATEGORY)
(ACCESSION NUMBER)	<i>63</i>	(NASA CR OR TMX OR AD NUMBER)
(PAGES)		

FACILITY FORM 602

## NATIONAL ADVISORY COMMITTEE FOR AERONAUTICS

## RESEARCH MEMORANDUM

SOME EFFECTS OF ROLL RATE ON THE LONGITUDINAL STABILITY

CHARACTERISTICS OF A CRUCIFORM MISSILE CONFIGURATION

AS DETERMINED FROM FLIGHT TEST FOR A

MACH NUMBER RANGE OF 1.1 TO 1.8

By Reginald R. Lundstrom and Hal T. Baber, Jr.

## SUMMARY

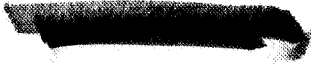
A model of a cruciform missile configuration having a low-aspect-ratio wing equipped with flap-type controls was flight tested in order to determine stability and control characteristics while rolling at about 5 radians per second. Comparison is made with results from a similar model which rolled at a much lower rate.

Results showed that, if the ratio of roll rate to natural circular frequency in pitch is not greater than about 0.3, the motion following a step disturbance in pitch essentially remains in a plane in space.

The slope of normal-force coefficient against angle of attack  $C_{N\alpha}$  was the same as for the slowly rolling model at  $0^\circ$  control deflection but  $C_{N\alpha}$  was much higher for the faster rolling model at about  $5^\circ$  control deflection. The slope of pitching-moment coefficient against angle of attack  $C_{m\alpha}$  as determined from the model period of oscillation was the same for both models at  $0^\circ$  control deflection but was lower for the faster rolling model at about  $5^\circ$  control deflection. Damping data for the faster rolling model showed considerably more scatter than for the slowly rolling model.

## INTRODUCTION

The Pilotless Aircraft Research Division of the Langley Laboratory has been conducting a series of free-flight tests through the use of



rocket-propelled models to investigate the general aerodynamic characteristics of a low-aspect-ratio cruciform missile configuration having trailing-edge flaps.

Longitudinal stability, control derivatives, and drag at subsonic and supersonic speeds as determined from a similar model which experienced very low rates of roll are presented in reference 1.

This paper presents longitudinal stability and control effectiveness for a model which is a replica, as regards configurational geometry and mass distribution, of the model for which data have been previously presented in reference 1. Since it was considered desirable to check the techniques of obtaining longitudinal stability derivatives of rolling missiles and to determine the general behavior of the missile when step inputs of the pitch control are applied, deflected ailerons were employed to roll the model approximately 5 radians per second at supersonic speeds. Comparisons are made throughout this report with the data obtained from the flight of the model of reference 1.

#### SYMBOLS

$a_n$	normal acceleration, ft/sec <sup>2</sup>
$a_t$	transverse acceleration, ft/sec <sup>2</sup>
$b$	exponential damping constant in $e^{-bt}$ , per second
$\bar{c}$	wing mean aerodynamic chord, ft
$d$	body diameter, ft
$g$	acceleration due to gravity, ft/sec <sup>2</sup>
$q$	dynamic pressure, lb/ft <sup>2</sup>
$A$	body cross-sectional area, sq ft
$C_N$	normal-force coefficient, $\frac{a_n}{g} \frac{W}{qA}$
$C_Y$	lateral-force coefficient, $\frac{a_t}{g} \frac{W}{qA}$

$C_R$	resultant-force coefficient corrected for trim, $\left[ (C_N - C_{N_{trim}})^2 + (C_Y - C_{Y_{trim}})^2 \right]^{1/2}$ where $C_{N_{trim}}$ and $C_{Y_{trim}}$ are determined using the method of reference 1
$I_X$	moment of inertia about X-axis, slug-ft <sup>2</sup>
$I_Y$	moment of inertia about Y-axis, slug-ft <sup>2</sup>
$I_Z$	moment of inertia about Z-axis, slug-ft <sup>2</sup>
$M$	Mach number, $V/V_C$
$P$	period of oscillation, sec
$S_w$	total area of rear lifting surfaces in one plane including body intercept, sq ft
$S_f$	trailing-edge-flap area in one plane, sq ft
$V$	velocity of model, ft/sec
$V_C$	speed of sound in air, ft/sec
$W$	model weight, lb
$\alpha$	angle of attack, deg
$C_{N_{trim}}$	value of $C_N$ when model is at pitch trim point
$C_{Y_{trim}}$	value of $C_Y$ when model is at yaw trim point
$\delta$	control deflection, deg
$\phi$	change in roll angle from the model roll attitude at time of previous pitch control step input, deg
$\dot{\phi}$	rate of roll, radians/sec
$\omega$	damped natural frequency in pitch, $2\pi/P$ , radians/sec

Derivatives:

$$C_{N\alpha} = \frac{\partial C_N}{\partial \alpha} \text{ per degree}$$

$$C_{m\alpha} = \frac{\partial C_m}{\partial \alpha} \text{ per degree}$$

## MODEL AND APPARATUS

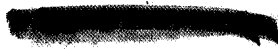
### Model Description

A sketch of the model arrangement is presented in figure 1 and a photograph of the model in figure 2. The fuselage, which had an overall fineness ratio of 12.16, consisted of a 6.40-inch-diameter cylindrical section, and a boattail rear section. The nose section of the model was a 2.25-inch-radius spherical segment and a parabolic section which provided a smooth transition from the spherical nose to the cylindrical section. The stationary forward lifting surfaces and the rear lifting surfaces which will be designated in this report as wings were mounted on the fuselage in an inline cruciform arrangement.

The steel wings of clipped delta plan form were flat plates with a thickness ratio of approximately 1.3 percent at the wing-body juncture. Leading and trailing edges were beveled with the leading edge being swept back  $76^\circ 23'$ . Wing panels in the horizontal plane were equipped with movable horn-balanced trailing-edge flaps as shown in figure 3. Panels in the vertical plane were identical to those in the horizontal plane with the exception that the trailing-edge controls were preset as ailerons to a differential deflection of  $0^\circ 35'$  to cause the model to roll at approximately 5 radians/second at supersonic speeds.

The flap-type controls in the lift plane, which were connected to move as a single unit, were programed in a continuous square-wave pattern by means of a hydraulic system and motor-driven valve. The two control positions were  $0^\circ$  and  $4.9^\circ$ , measured with respect to the wing plane.

Physical characteristics of the model are presented in the following table:



W, lb . . . . .	141.50
Center of gravity, rear of station 0 . . . . .	46.00
$I_x$ , slug-ft <sup>2</sup> . . . . .	0.312
$I_y$ , slug-ft <sup>2</sup> . . . . .	22.28
$I_z$ , slug-ft <sup>2</sup> . . . . .	22.28
d, ft . . . . .	0.533
A, sq ft . . . . .	0.223
$S_w$ , sq ft . . . . .	3.250
$S_f$ , sq ft . . . . .	0.267
$\bar{c}$ , ft . . . . .	2.540

### Instrumentation

The model was equipped with an NACA eight-channel telemeter which transmitted a continuous record of normal, transverse, and longitudinal acceleration, angle of attack, rate of roll, control deflection, total pressure, and static pressure. Angle of attack was measured by a free-floating vane mounted on a sting which protruded from the nose of the model. Rolling velocity was measured by a rate gyro. Total pressure was obtained by a total-pressure tube extended from the fuselage ahead of the wings and in a plane 45° to the two wing planes. A static-pressure orifice was located on the cylindrical section of the fuselage ahead of the wings.

Velocity was measured by a CW Doppler velocimeter and agreed closely with that obtained through the use of the total pressure. The model's position in space was determined by an NACA modified SCR 584 tracking radar set. Atmospheric temperature and pressure were measured by a radiosonde which was released immediately after the flight.

### TEST TECHNIQUE

The model, which was launched from a zero-length mobile launcher at a 45° elevation angle, was boosted to supersonic velocity by two 6-inch-diameter solid-propellant rocket motors which together delivered approximately 12,000 pounds of thrust for 3 seconds. After model and booster separated, the model was disturbed in pitch by a programed square-wave deflection of the trailing-edge flaps. Transient responses to the step input of the control surface were continuously recorded in the form of time histories as the model decelerated through the Mach number range.



## PRECISION OF DATA

## Corrections

Velocity data as obtained by the CW Doppler velocimeter were corrected for flight-path curvature and wind effect at altitude. The magnitudes and directions of these winds were determined by tracking the radiosonde balloon.

In order to obtain the angle of attack at the center of gravity, the angle of attack measured at the nose was corrected for model pitching velocity by the method of reference 2. Angle-of-attack corrections due to combined yaw angle and roll rate were investigated and found to be negligible.

## Accuracy

On the basis of the accuracies of the instrumentation and dynamic pressure, the maximum possible errors in  $M$ ,  $\alpha$ ,  $\delta$ , and  $C_N$  are listed as incremental values. It should be reiterated here that  $C_N$  is based on body cross-sectional area.

M	Limit of accuracy of -			
	M	$\alpha$	$\delta$	$C_N$
1.10	$\pm 0.01$	$\pm 0.50$	$\pm 0.10$	$\pm 0.30$
1.80	$\pm 0.02$	$\pm 0.50$	$\pm 0.10$	$\pm 0.09$

These errors, dependent upon telemeter and radar precision, are essentially systematic in nature. From a consideration of previous experience, probable errors are 50 percent less than those just quoted. Parameters dependent upon differences in measured quantities or slopes such as  $C_{N\alpha}$  are more accurately determined than the previously mentioned errors would indicate.

## RESULTS AND DISCUSSION

The Reynolds number per foot for this test varied from  $12.16 \times 10^6$  at  $M = 1.75$ , to  $6.29 \times 10^6$  at  $M = 1.10$ . The atmospheric data as well

as the mass and moment of inertia are almost identical for the present model and model 2 of reference 1. No data are presented below a Mach number of 1.1 because the instrument limits were exceeded, probably due to the fact that the model was near roll resonance ( $\dot{\phi}/\omega = 1$ ) in this range.

The control motion from  $\delta = 0^\circ$  to  $\delta = 4.9^\circ$  was very rapid, being less than 0.02 second. The roll displacement of the model over this time was usually less than  $7^\circ$ .

Even though the roll rate averages about 5 radians per second the wing-tip helix angle is very small. For a roll rate of 5 radians per second the wing tip helix angle is about  $0.2^\circ$  at  $M = 1.1$  and  $0.1^\circ$  at  $M = 1.75$ .

#### Time Histories

The time histories of  $\delta$ ,  $C_N$ ,  $C_Y$ , and  $\dot{\phi}$  as obtained from the flight test are shown in figure 4. As may be seen in figure 4, the  $C_N$  trace is so irregular that no period or damping constant could possibly be obtained. Even though the model was disturbed only in pitch, quite large and irregular values of side force were induced. Figure 4 also indicates that the steady-state roll rate at  $\delta = 0$  is much greater than when  $\delta = 4.9^\circ$ . This was also the case with the much slower rolling model of reference 1. This means that either the roll damping was increased, because the roll caused a change in the downwash pattern over the wing, or the aileron effectiveness was reduced because of the higher angle of attack associated with the  $4.9^\circ$  control deflection. In figure 4 the oscillation on the roll-rate trace immediately following control motion from  $0^\circ$  to  $4.9^\circ$  is evidence of rolling moment due to combined angle of attack and sideslip and is more noticeable at the lower Mach numbers.

Reduction of the data was carried out by use of the method of reference 1 which consisted of plotting  $C_N$  against  $C_Y$  for each of the control pulses and, after accounting for the trim as well as possible, developing time histories of  $C_R$ . Because reference 1 showed that at very low roll rates the damped harmonic motion effectively took place in the plane in space in which the step disturbance was created, it was decided to determine whether that condition applied also to this model which rolled at a much higher rate. For this analysis an axis system was used similar to that referred to in reference 3 as "pseudo-stability axes" for missiles having  $90^\circ$  rotational symmetry. This is the same as a body-axis system except that the Y- and Z-axes do not roll with the model. For the analysis considered here the position of the XZ plane coincides



with the XZ plane of a body-axis system at the instant the control surface is given the step input but holds this position in space (except for translations of the model in which case the whole axis system translates) during the analysis of that entire pulse. The roll position of the model at any time during a pulse as measured from its roll attitude at the beginning of that pulse was determined by integration of the measured roll rate. The values of  $C_N$  and  $C_Y$  from the body-axis system were then converted to  $C_N$  and  $C_Y$  of the pseudo-stability axis system, designated  $C_{N_S}$  and  $C_{Y_S}$ , respectively, by the following relationships:

$$C_{N_S} = C_N \cos \phi - C_Y \sin \phi$$

$$C_{Y_S} = C_N \sin \phi + C_Y \cos \phi$$

If the damped harmonic motion resulting from the step control input remained in a plane, it must be in the XZ plane of the pseudo-stability axis system. For this condition if the model had perfect symmetry such that it would trim out at  $C_N = 0$ ,  $C_Y = 0$ ,  $C_{Y_S}$  would always be zero.

If, however, the model had asymmetry (such as misalignment or deflected control surfaces) a plot of  $C_{Y_S}$  against  $\phi$  would be a sine wave having its maxima when the asymmetry is in the XY plane and being zero when the asymmetry is in the XZ plane. Sample plots of  $C_{Y_S}$  against  $\phi$  are presented in figure 5. The values of  $C_{N_{trim}}$  and  $C_{Y_{trim}}$  are the values of  $C_{Y_S}$  at  $\phi = 90^\circ$  and  $\phi = 0^\circ$ , respectively. The irregularity in the curve of  $C_{Y_S}$  against  $\phi$  is evidence that the actual motion is not entirely in the XZ plane. This irregularity became more pronounced as the Mach number decreased and thus increased the inaccuracies in determining  $C_{N_{trim}}$  and  $C_{Y_{trim}}$ .

The term  $C_{N_S}$  is made up partly of  $C_N$  due to asymmetry and partly of  $C_N$  due to the pitching motion. The value of  $\Delta C_{N_S}$ , which is that part of  $C_{N_S}$  due to the pitching motion, was determined by the following relationship:

$$\Delta C_{N_S} = (C_N - C_{N_{trim}}) \cos \phi - (C_Y - C_{Y_{trim}}) \sin \phi$$

Values of  $C_R$  and  $\Delta C_{N_S}$  against time are shown in figure 6 for three typical pulses. The solid curve was obtained by use of the method of reference 1 and the circled points were obtained by assuming the response to the step input was entirely in the XZ plane of the pseudo-stability

axis system. The agreement was good for the first four pulses where  $\dot{\phi}/\omega$  was less than about 0.3. Two of these pulses are shown in figure 6(a) and figure 6(b). For the remaining pulses, however, of which figure 6(c) is typical, the agreement was rather poor. The greater amplitude of oscillation and lower damping constant at the lower Mach numbers caused much more energy of the pitching oscillation from the previous pulse to remain when the pitch controls moved abruptly to the new position. As the Mach number decreased, the roll rate increased somewhat so that the model rolled through about  $270^\circ$  during each pulse. Rolling through  $90^\circ$  or  $270^\circ$  per pulse means that the space position of the XY plane (pseudo-stability axis system) for one pulse had about the same orientation as the XZ plane from the previous pulse. This prevented any possibility of the pitching motion remaining in the XZ plane. This could have been avoided by decreasing the frequency of the pulses so that the oscillation which resulted from one pulse would have decayed to a small amplitude before the next pulse started. However, existing theory on rolling missiles such as reference 4 does indicate that at these higher values of  $\dot{\phi}/\omega$  the pitching motion created by the step input would move appreciably out of the XZ plane even though the pitching motions from the previous pulse were completely damped.

#### Normal Force Due to Angle of Attack

Typical plots of  $C_N$  against  $\alpha$  are presented in figure 7. The plots show a lower slope for values of  $\alpha$  between  $0^\circ$  and  $-2^\circ$  than at values of  $\alpha$  more negative than  $-3^\circ$ . Unpublished wind-tunnel data also show this nonlinearity as do the data from the model of reference 1. Since  $\beta$  was not measured on this model, it was not possible to make plots of  $C_Y$  against  $\beta$  or  $C_R$  against resultant angle. Average slopes were measured at  $\alpha \approx 0^\circ$  and  $\alpha \approx -4^\circ$  and are presented as symbols in figure 8. The solid lines in figure 8 are values of  $C_{N_\alpha}$  obtained from the model of reference 1. It should be noted that  $C_{L_\alpha}$  is presented in reference 1 instead of the plot of  $C_{N_\alpha}$  presented here. Figure 8 shows very good agreement for  $C_{N_\alpha}$  between the two models at  $\alpha \approx 0^\circ$  and  $\delta = 0^\circ$ , but considerably higher values of  $C_{N_\alpha}$  for the present rolling model than for the slowly rolling model of reference 1 when  $\alpha \approx -4^\circ$  and  $\delta = 4.9^\circ$ . Inspection of the data from the model reported in reference 1 showed that  $C_{N_\alpha}$  was the same value at  $\alpha \approx 0^\circ$  whether  $\delta = 0^\circ$  or  $\delta = 4.8^\circ$ . However, as may be seen in figure 8 for the faster rolling model at  $\alpha \approx 0^\circ$ ,  $C_{N_\alpha}$  is much greater when  $\delta = 4.9^\circ$  than when  $\delta = 0^\circ$ . Because the roll rates are greater at the pulses when  $\delta = 0^\circ$  where the agreement between the two models is very good it is believed that the contribution of the Magnus force coefficients to the total  $C_N$  is small



and that neglect of these Magnus forces in reducing the data is not the reason for the greater value of  $C_{N\alpha}$  obtained for the faster rolling model. The greater  $C_{N\alpha}$  appears therefore to be a direct result of the combination of asymmetry (due to the control deflection) and roll rate.

#### Pitching Moment Due to Angle of Attack

The plots of  $C_R$  against time shown in figure 6 were typical of damped harmonic motion. The damped natural frequency variation with Mach number is shown in figure 9. The pitching-moment derivative  $C_{m\alpha}$  was derived from the faired values of  $\omega$  and is presented as the symbols of figure 10. The solid lines on figure 10 are taken from reference 1. The agreement is very good for the  $\delta = 0^\circ$  pulses, but the values of  $C_{m\alpha}$  for the  $\delta = 4.9^\circ$  pulses are usually much less from the model with the greater roll rate. The  $C_{m\alpha}$  values for the first pulse ( $\delta = 4.9^\circ$ ,  $M = 1.73$ ) appear to be approximately on an extrapolation of the curve from reference 1. Figure 4 shows that the roll rate is much lower during this pulse than during any other pulse. If the same reasoning as for  $C_{N\alpha}$  that the Magnus terms are probably small because of the good agreement at  $\delta = 0^\circ$  is used, the low values of  $C_{m\alpha}$  obtained for the rolling model must be due to a combination of asymmetry and roll rate.

#### Damping

The exponential damping constant  $b$  is presented in figure 11 as a function of Mach number. The solid lines are taken from reference 1. Direct comparison of damping constant for the two models is possible because of the similarity of the mass characteristics of the two models and the similar atmospheric conditions experienced during their flights. The test points for the faster rolling model are widely scattered. It should be noted however that, if the values of  $b$  over a pulse had been averaged instead of plotted as individual points, the agreement would have looked fairly good. The test points indicate that the damping is greater at the greater amplitudes but this may not be true. The technique used for determining the damping assumes that the model passes through  $C_{N_{trim}}$  and  $C_{Y_{trim}}$  at the same instant. When this is not the case it is virtually impossible to determine the actual trim point, especially with the limited number of cycles available at the low Mach numbers. This uncertainty of the trim is without doubt a major cause of the scatter of test points on figure 11.

### Control Effectiveness

The effectiveness of the controls in producing lift is presented in figure 12. Because of the variation in normal-force trim over a pulse during the present test it was necessary to use methods of determining  $C_{N\delta}$  different from those used in reference 1. One method used was to take the  $C_N$  value at  $\alpha = 1^\circ$  (obtained from plots of  $C_N$  against  $\alpha$ ) for  $\delta = 0^\circ$  and  $\delta = 4.9^\circ$  and plot it against  $M$ , a curve being faired for each of the  $\delta$  positions. The difference between the two curves is the  $C_N$  due to  $\delta = 4.9^\circ$ . The second method involved the use of  $C_N$  values just before and after the control surface changed position with precautions taken to keep within the frequency response limitations of the accelerometer. The  $\Delta C_N / \Delta \delta$  was then obtained from the relationship:  $\Delta C_{N\delta} \Delta \delta = \Delta C_N - C_{N\alpha} \Delta \alpha$ , where  $\Delta C_N$  and  $\Delta \alpha$  refer to the change in  $C_N$  or  $\alpha$  between the point before and point after the control surface motion. The points were chosen so that  $\Delta \alpha$  was very small in order to obtain better accuracy for  $\Delta C_N / \Delta \delta$ . Test points for these two methods are shown in figure 12 and the agreement between them is good. Agreement with values of  $\Delta C_N / \Delta \delta$  from reference 1 is fair and would indicate no great variation of  $\Delta C_N / \Delta \delta$  due to roll rate.

Variation of control-surface pitching effectiveness with Mach number is presented in figure 13. This was obtained by multiplying values of  $\Delta C_N / \Delta \delta$  by the distance from the center of gravity to the control surface hinge line in body diameters. No comparison is made with reference 1 since the values on figure 13 are merely the values on figure 12 multiplied by a constant.

### CONCLUSIONS

Results from the flight test of a cruciform missile configuration which rolled about 5 radians per second when compared with the results from a similar model which rolled at a much lower rate indicated:

1. Stability derivatives may be obtained from a symmetrical rolling model where  $\dot{\phi} / \omega$  (that is,  $\frac{\text{Roll rate}}{\text{Pitch frequency}}$ ) is about 0.3 or less but damping data will have considerably more scatter than for a nonrolling model.
2. It would facilitate reduction of stability data if the oscillations from one disturbance are allowed to decay to a small amplitude before the next disturbance occurs.

3. The oscillations will essentially take place in a plane in space if the input is rapid and the value of  $\dot{\phi}/\omega$  low.

4. The value of the normal-force derivative  $C_{N\alpha}$  for the faster rolling model was the same as for the slower rolling model at  $0^\circ$  control deflection but was much greater for the faster rolling model at  $4.9^\circ$  control deflection.

5. The value of the pitching-moment derivative  $C_{m\alpha}$  as obtained from the period of the oscillations was the same for the faster rolling model as for the slower rolling model at  $0^\circ$  control deflection but was less for the faster rolling model at  $4.9^\circ$  control deflection.

6. Roll rate causes no great change in the normal force due to elevator deflection.

Langley Aeronautical Laboratory,  
National Advisory Committee for Aeronautics,  
Langley Field, Va., December 2, 1955.

#### REFERENCES

1. Baber, Hal T., Jr., and Moul, Martin T.: Longitudinal Stability and Control Characteristics As Determined by the Rocket-Model Technique for an Inline, Cruciform, Canard Missile Configuration With a Low-Aspect-Ratio Wing Having Trailing-Edge Flap Controls for a Mach Number Range of 0.7 to 1.8. NACA RM L54B12, 1955.
2. Mitchell, Jesse L., and Peck, Robert F.: An NACA Vane-Type Angle-of-Attack Indicator for Use at Subsonic and Supersonic Speeds. NACA TN 3441, 1955. (Supersedes NACA RM L9F28a.)
3. Charters, Alex C.: The Linearized Equations of Motion Underlying the Dynamic Stability of Aircraft, Spinning Projectiles, and Symmetrical Missiles. NACA TN 3350, 1955.
4. Nicolaidis, John D.: On the Free Flight Motion of Missiles Having Slight Configurational Asymmetries. Rep. No. 858, Ballistic Res. Labs., Aberdeen Proving Ground, June 1953.

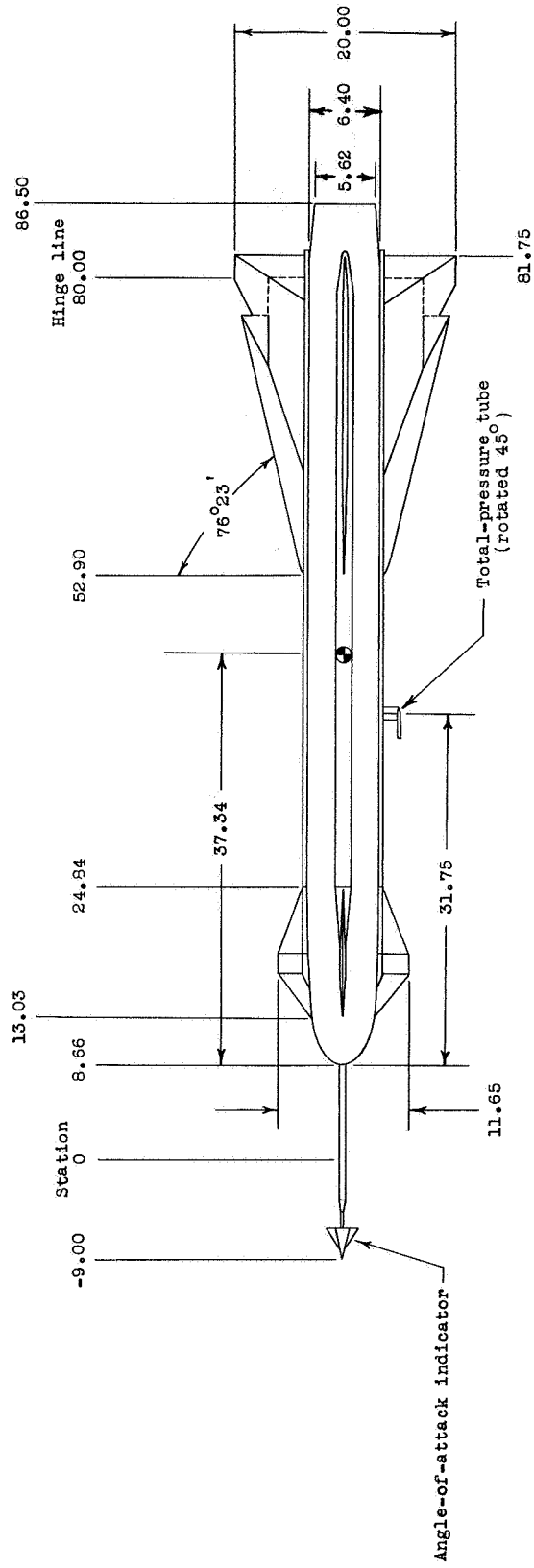
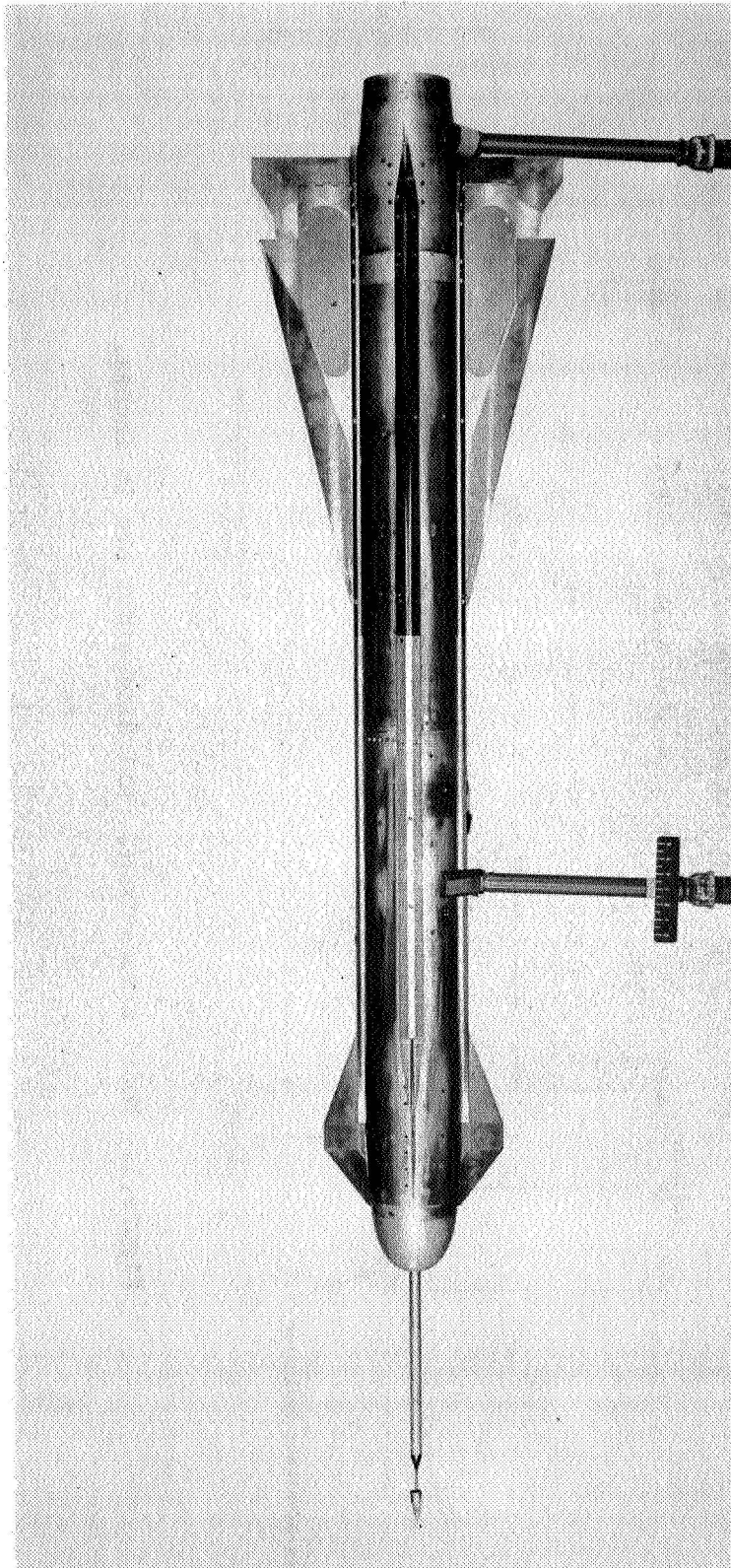


Figure 1.- Model arrangement. All dimensions are in inches.



L-87718.1

Figure 2.- Side view of the model.

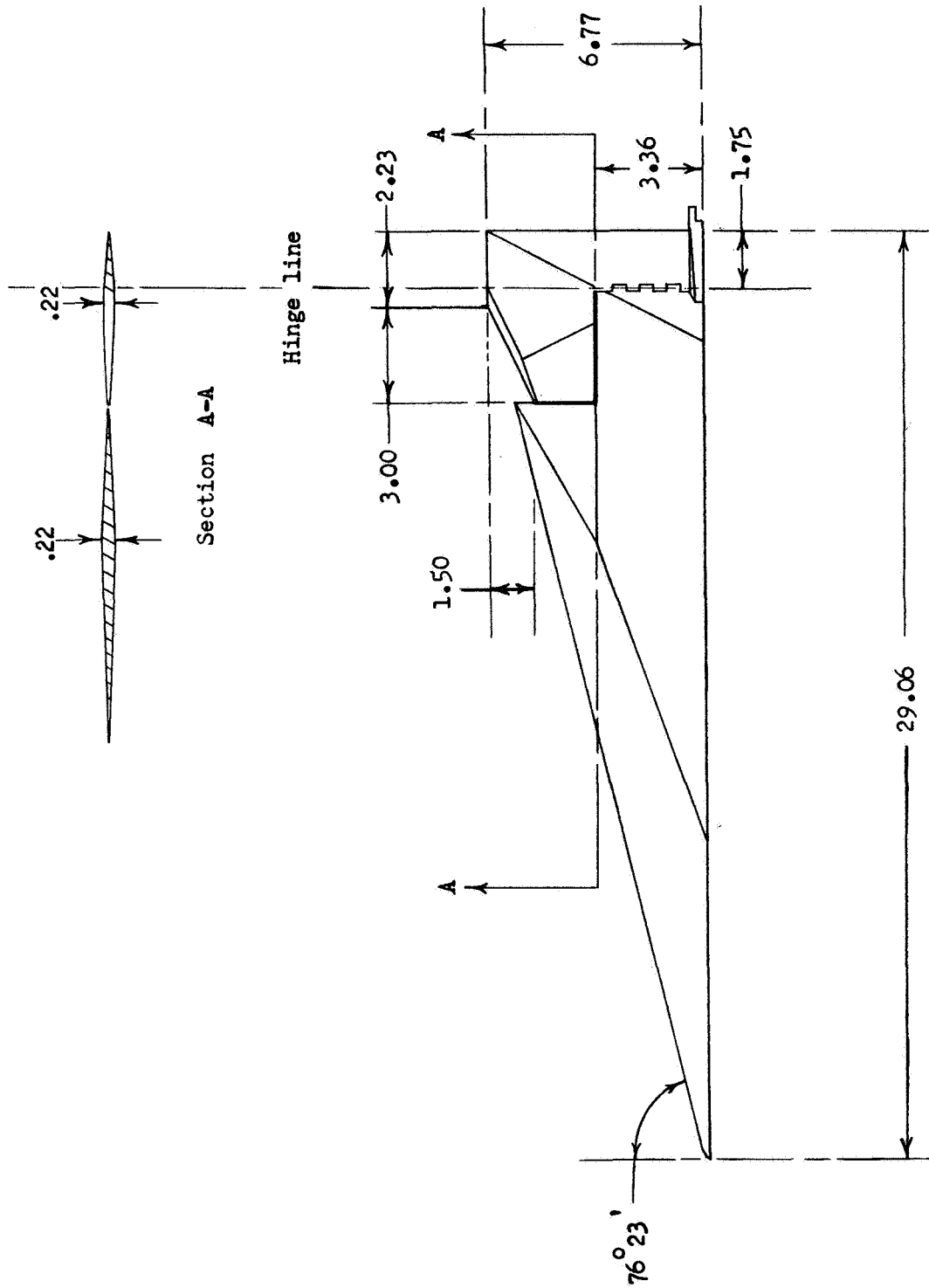
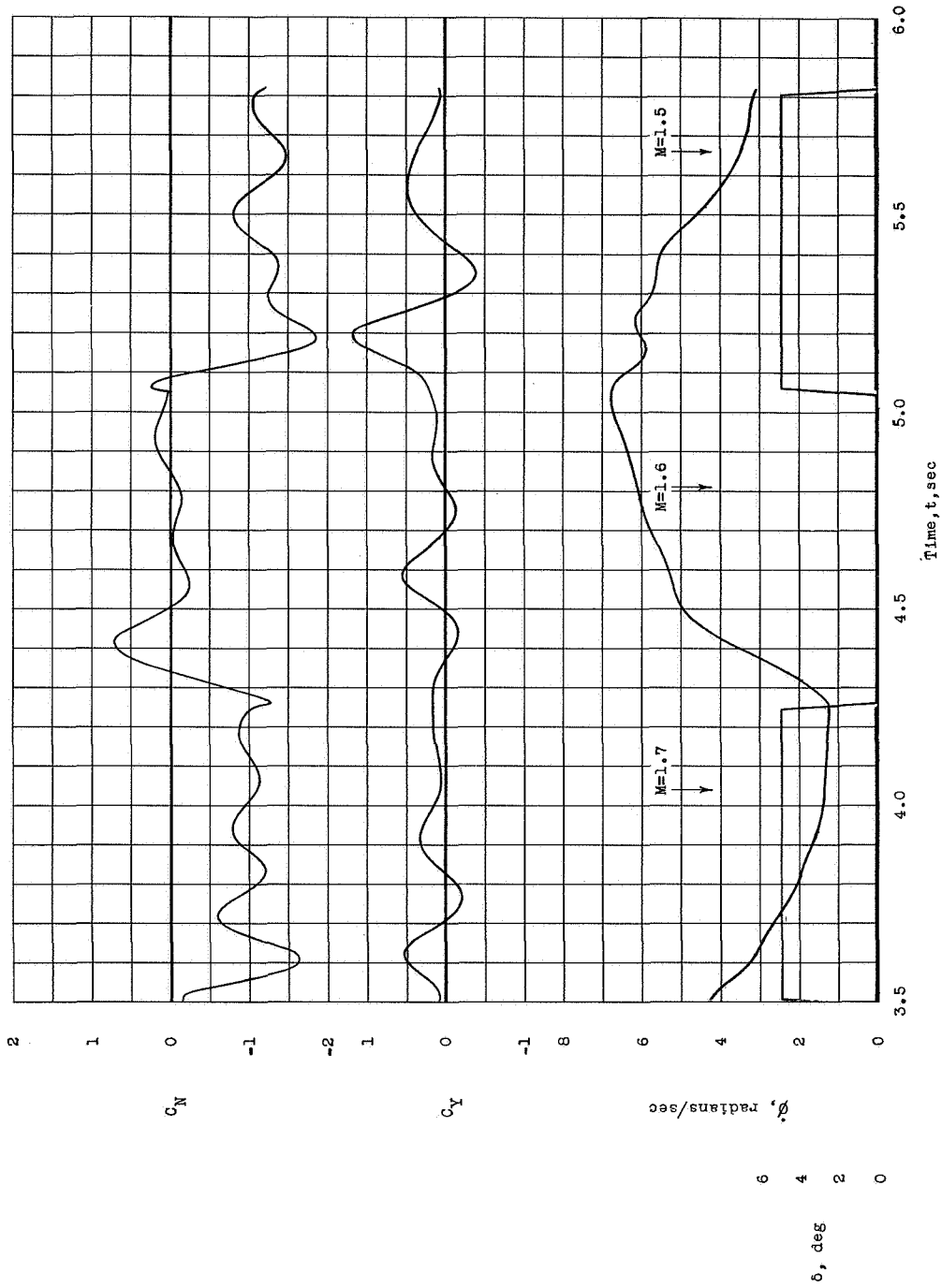
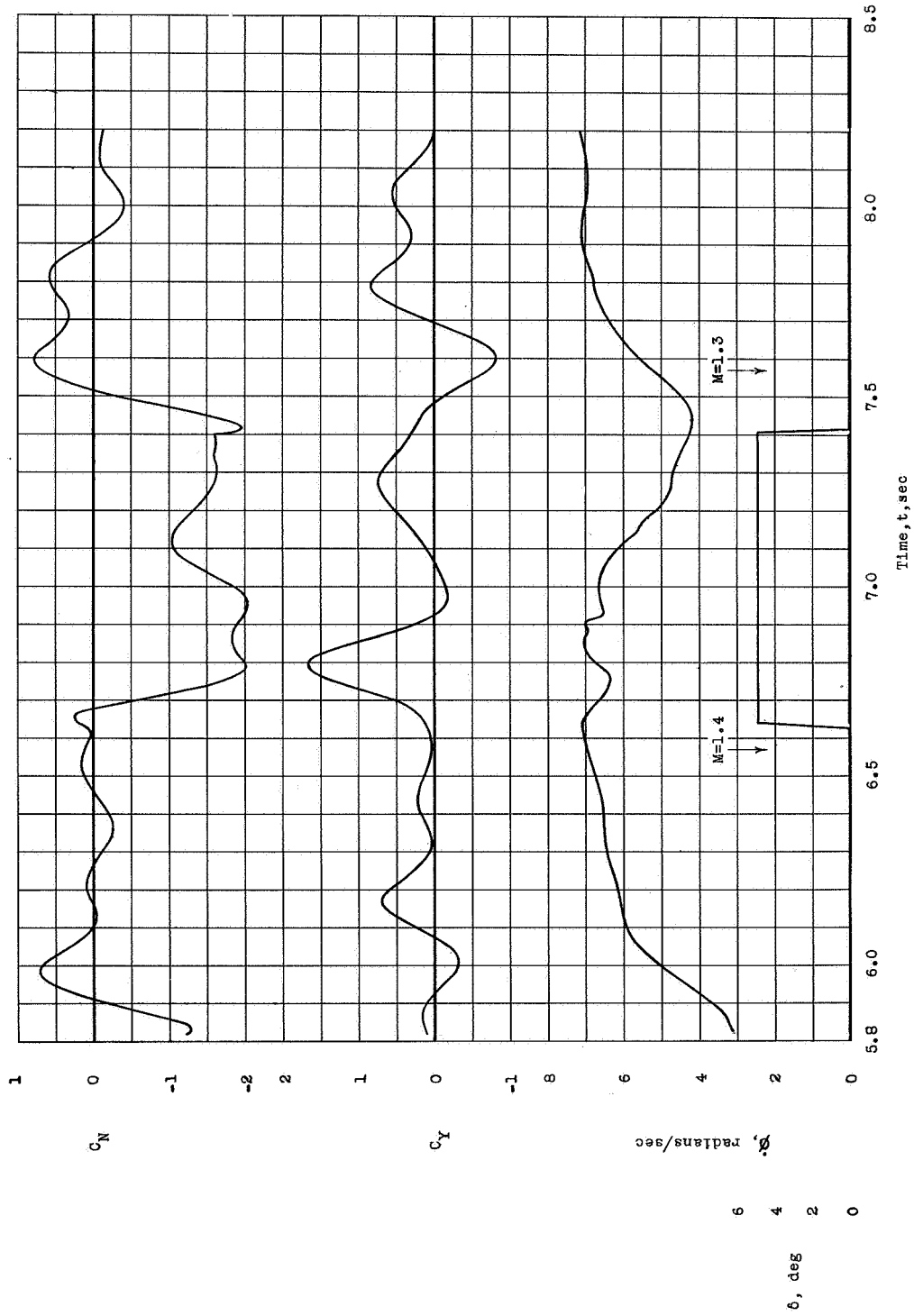


Figure 3.- Wing and control detail. All dimensions are in inches.



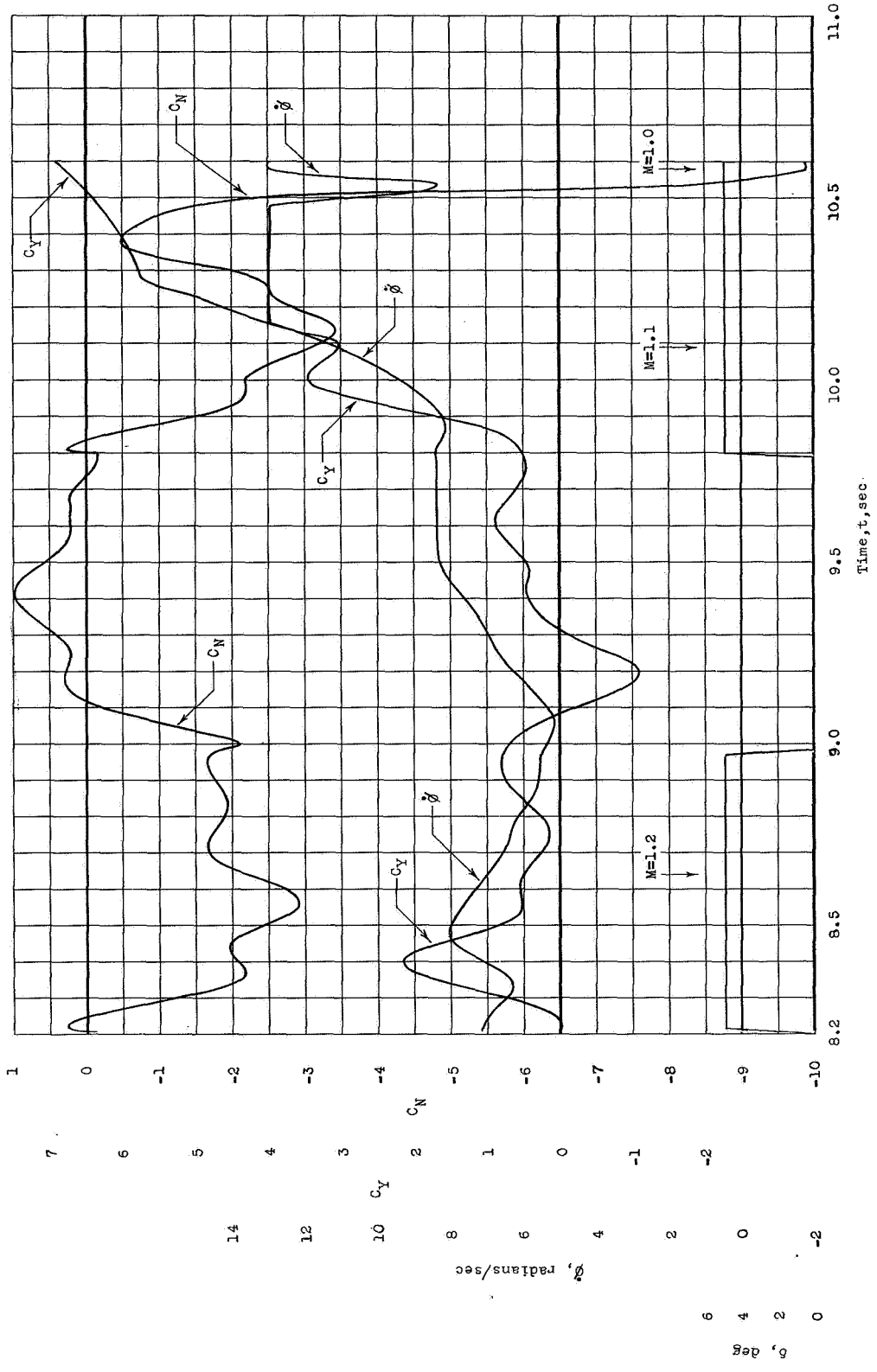
(a) Pulses 1, 2, and 3.

Figure 4.- Time histories.



(b) Pulses 4, 5, and 6.

Figure 4.- Continued.



(c) Pulses 7, 8, and 9.

Figure 4.- Concluded.

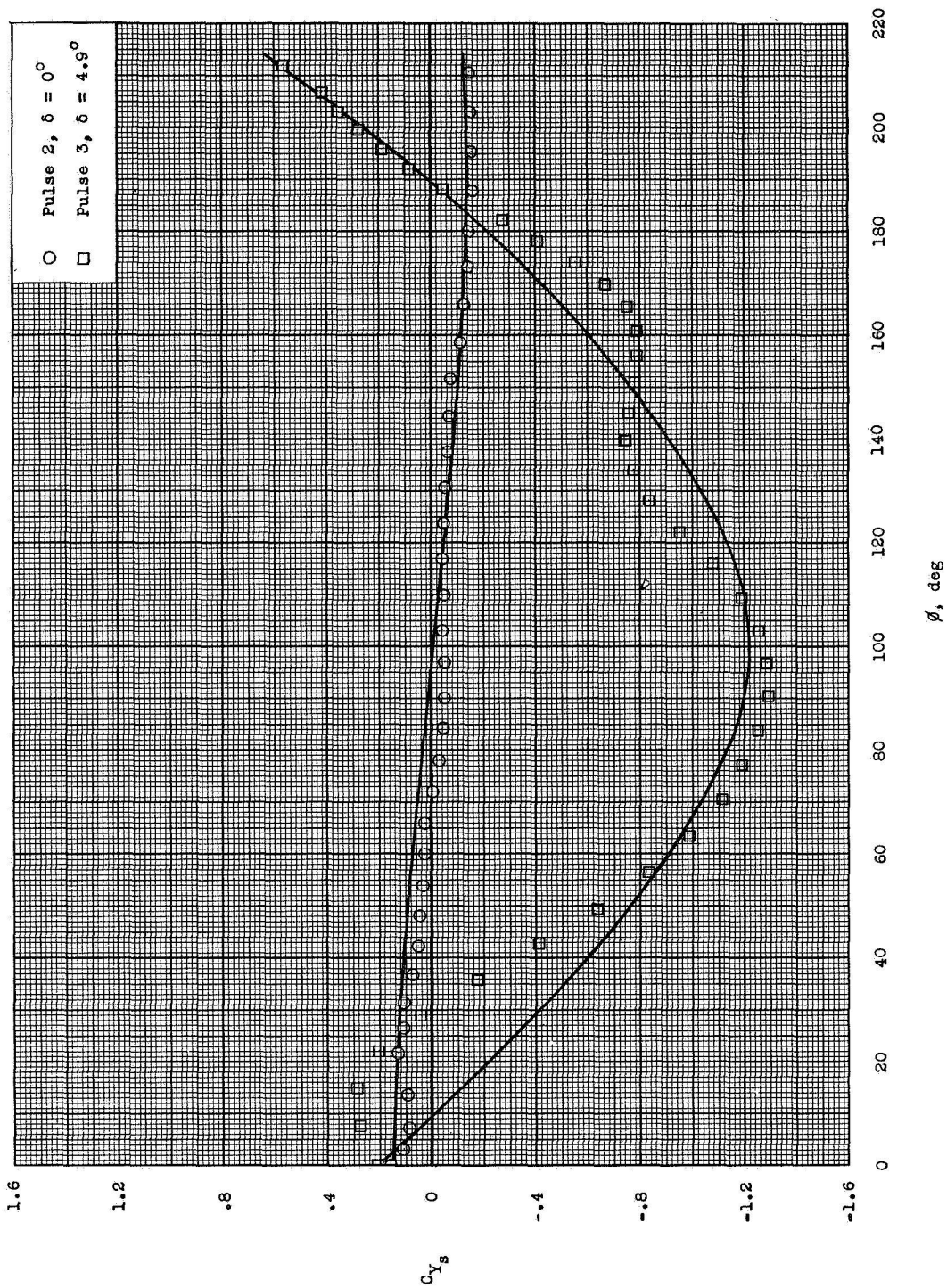
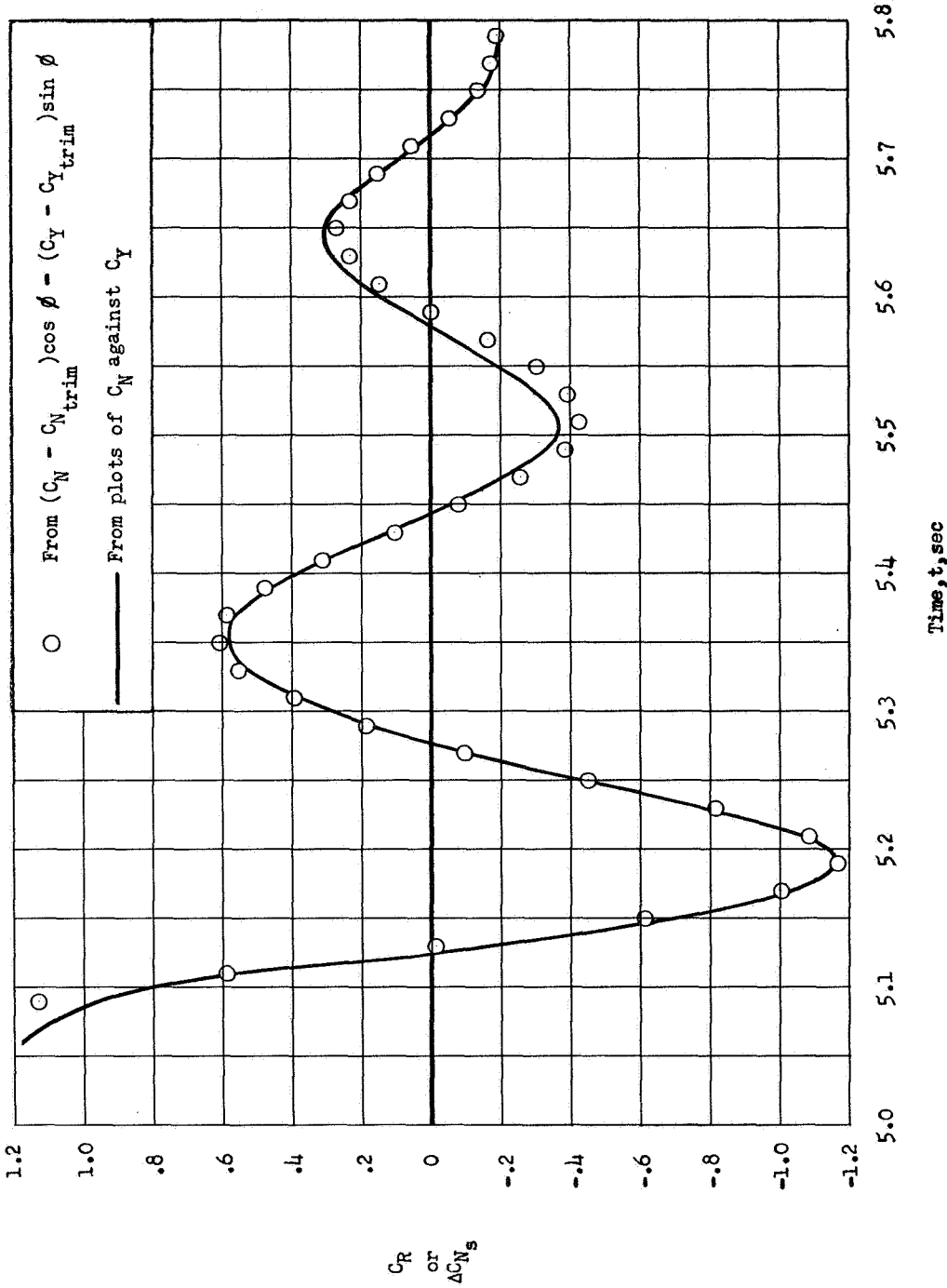
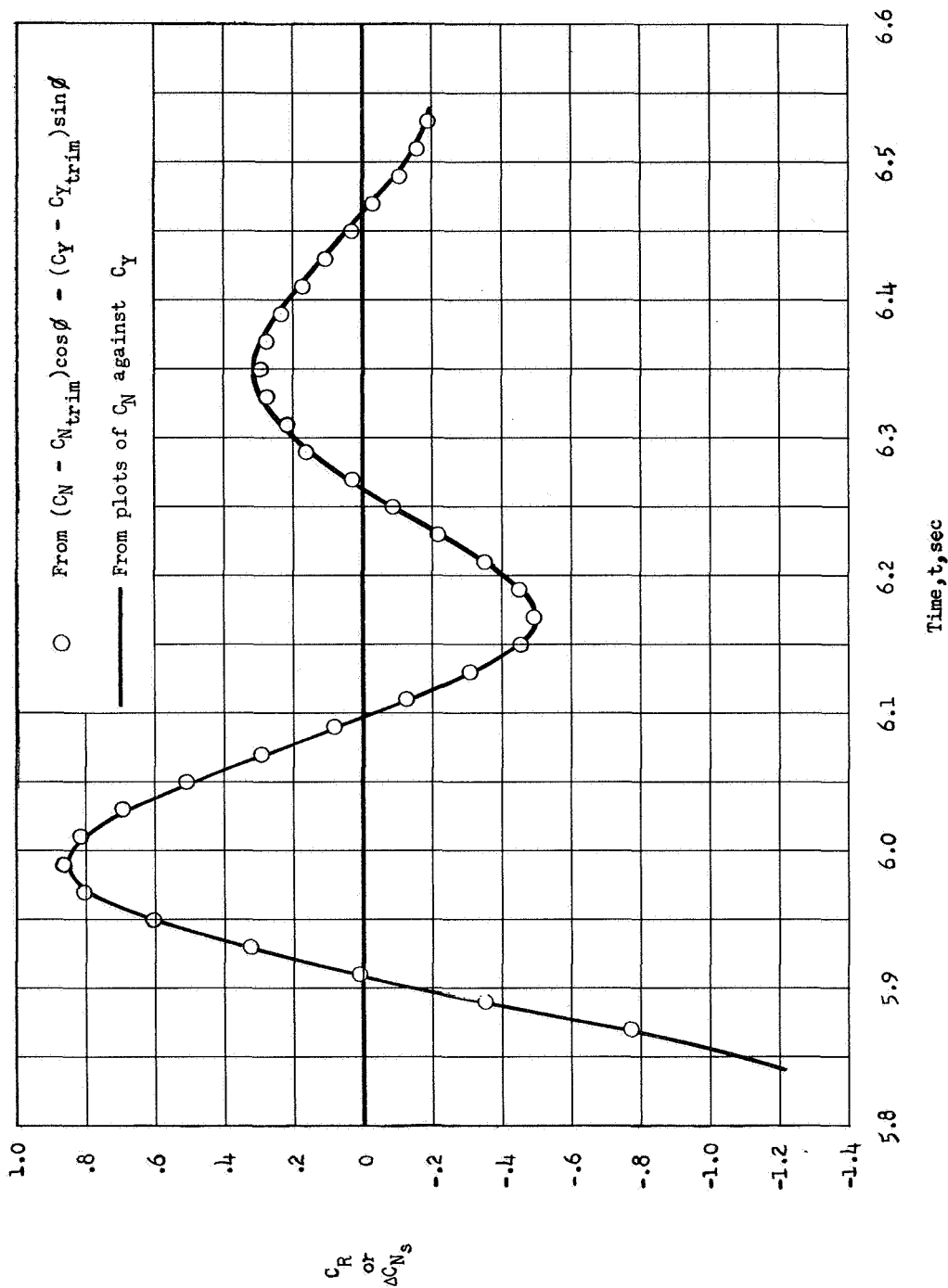


Figure 5.- Variation of lateral-force coefficient, as measured along pseudo-stability axis, with roll angle.

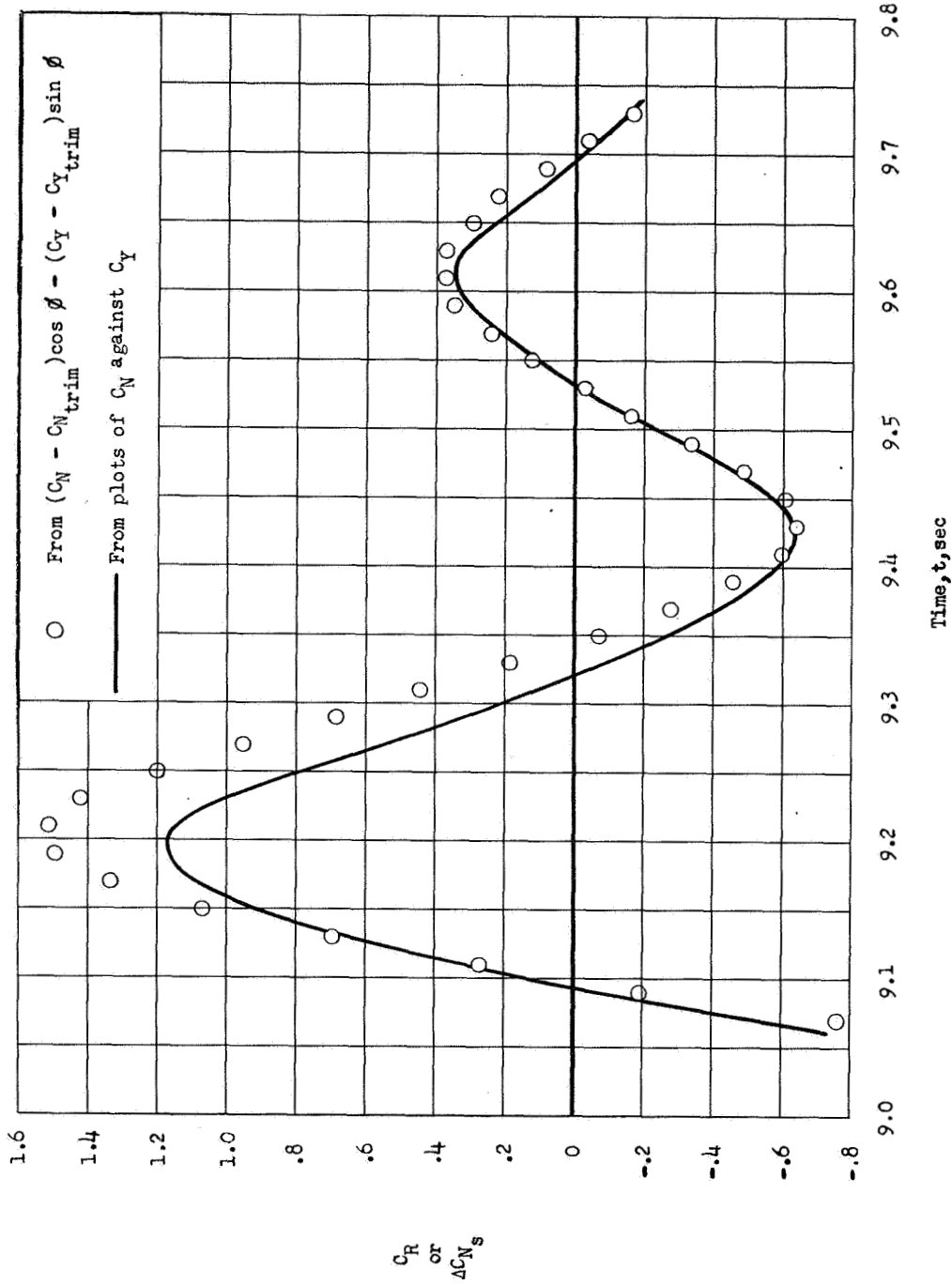


(a) Pulse 3;  $\delta = 4.9^\circ$ .

Figure 6.- Sample resultant-force-coefficient time histories.

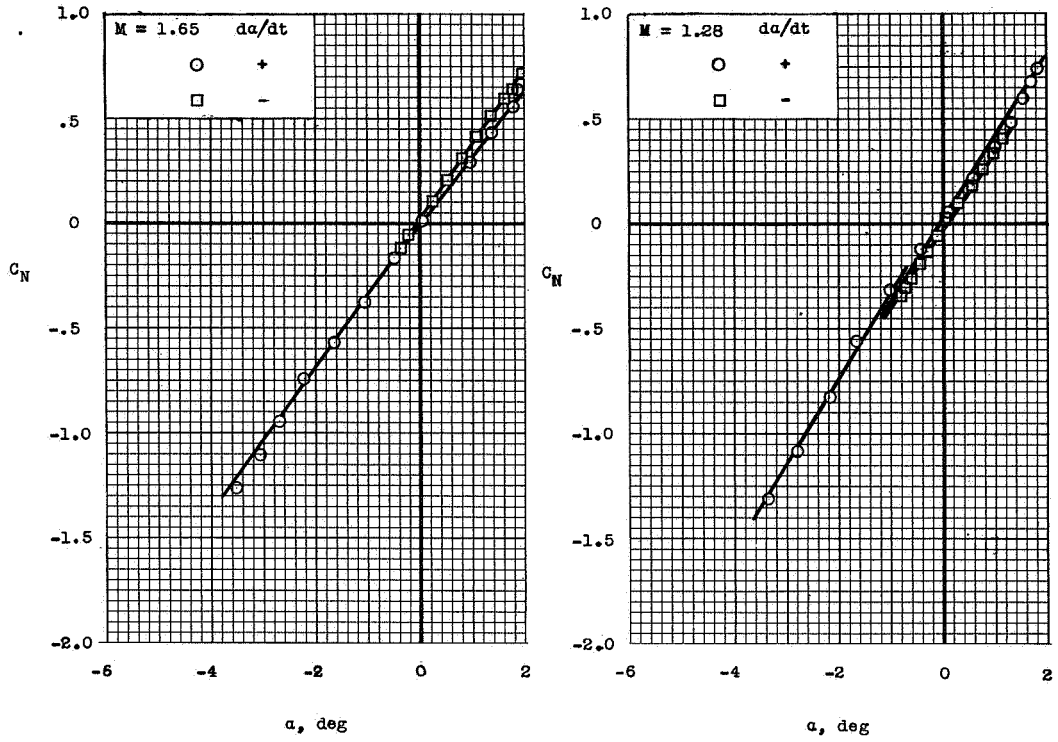


(b) Pulse 4;  $\delta = 0^\circ$ .  
Figure 6.- Continued.

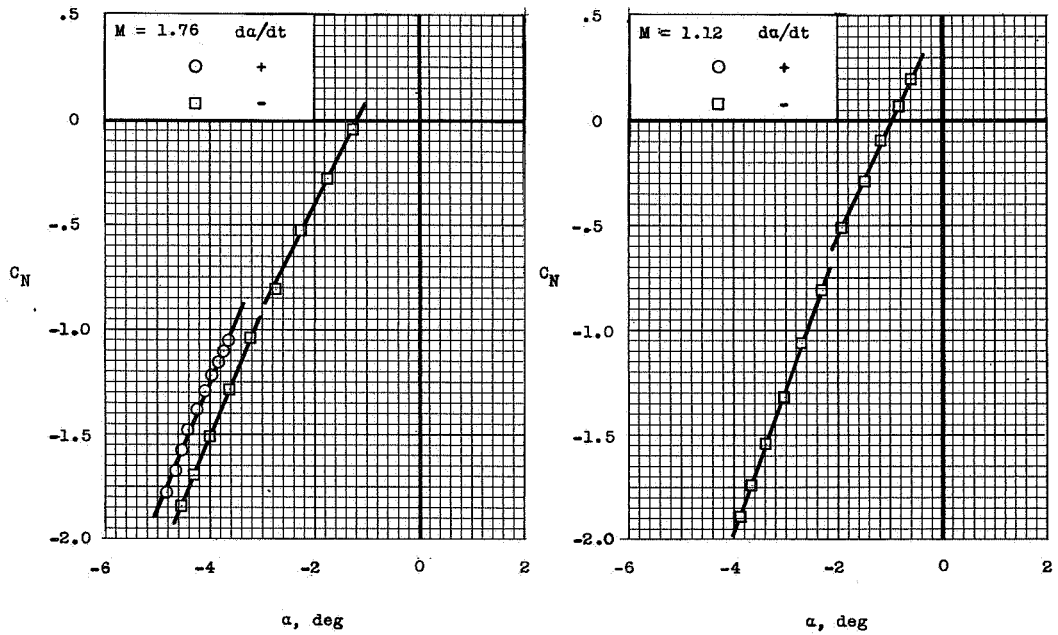


(c) Pulse 8;  $\delta = 0^\circ$ .

Figure 6.- Concluded.



(a)  $\delta = 0^\circ$ .



(b)  $\delta = 4.9^\circ$ .

Figure 7.- Variation of normal-force coefficient with angle of attack.

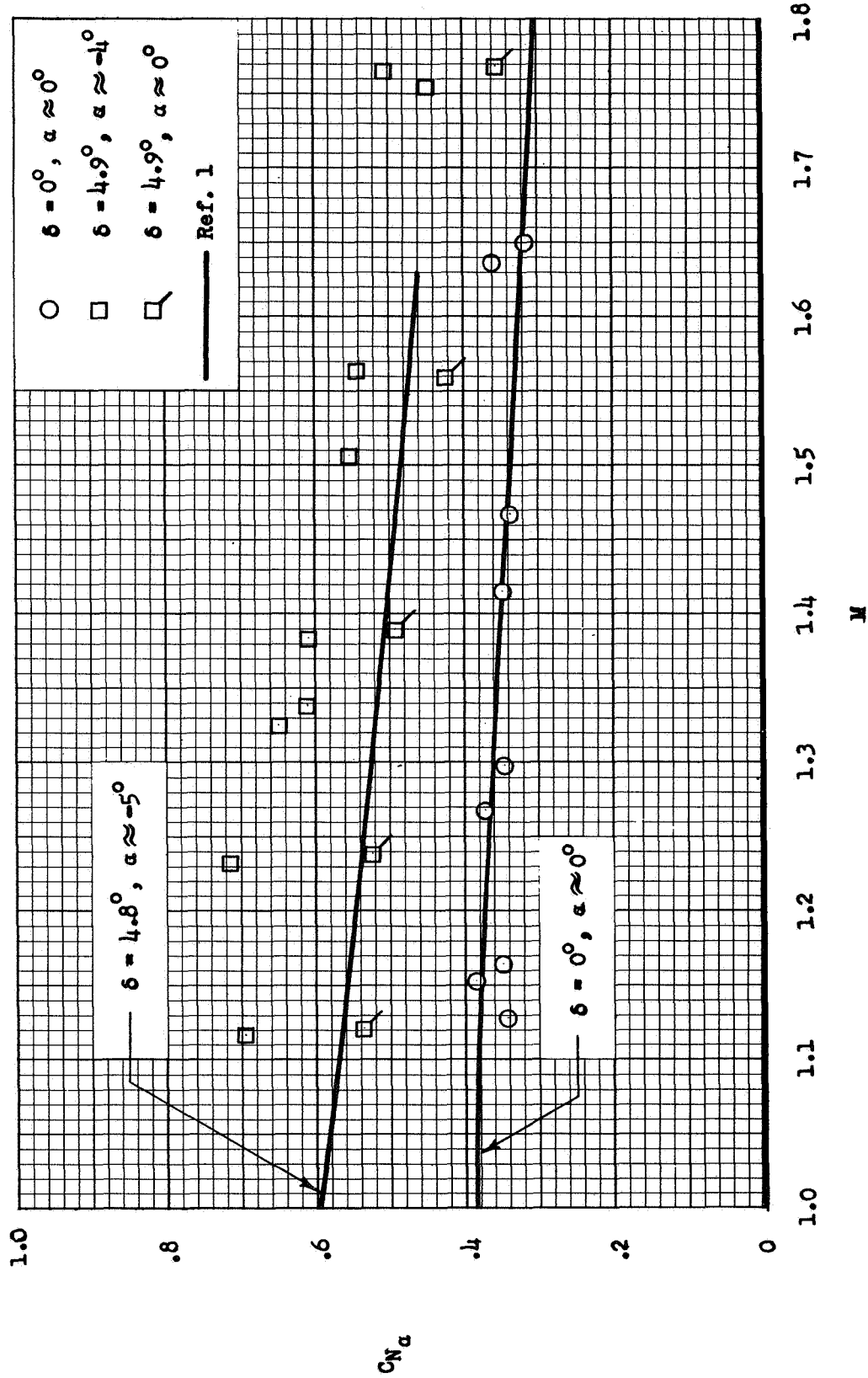


Figure 8.- Variation of normal-force-curve slope with Mach number.

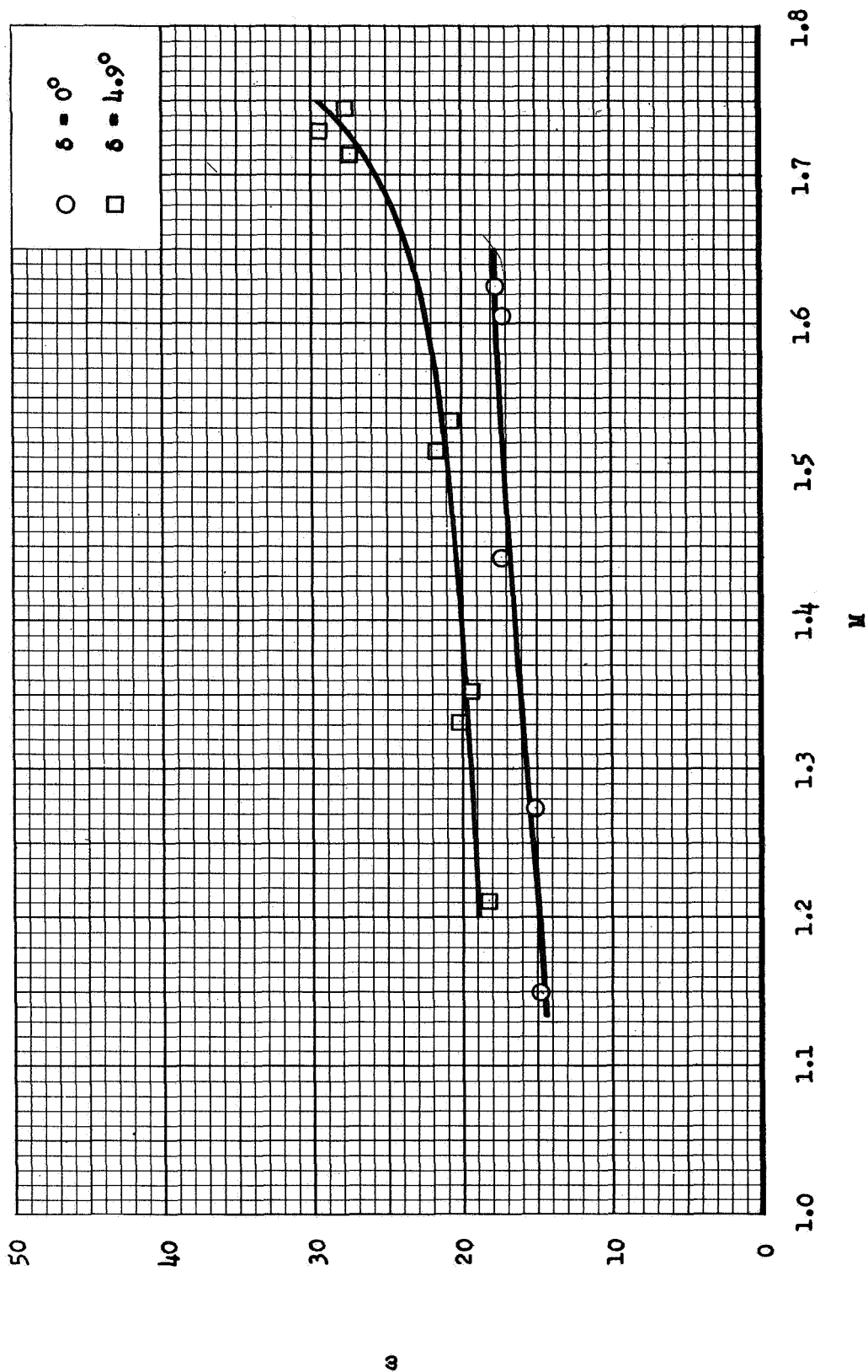


Figure 9.- Variation of damped natural frequency in pitch with Mach number.

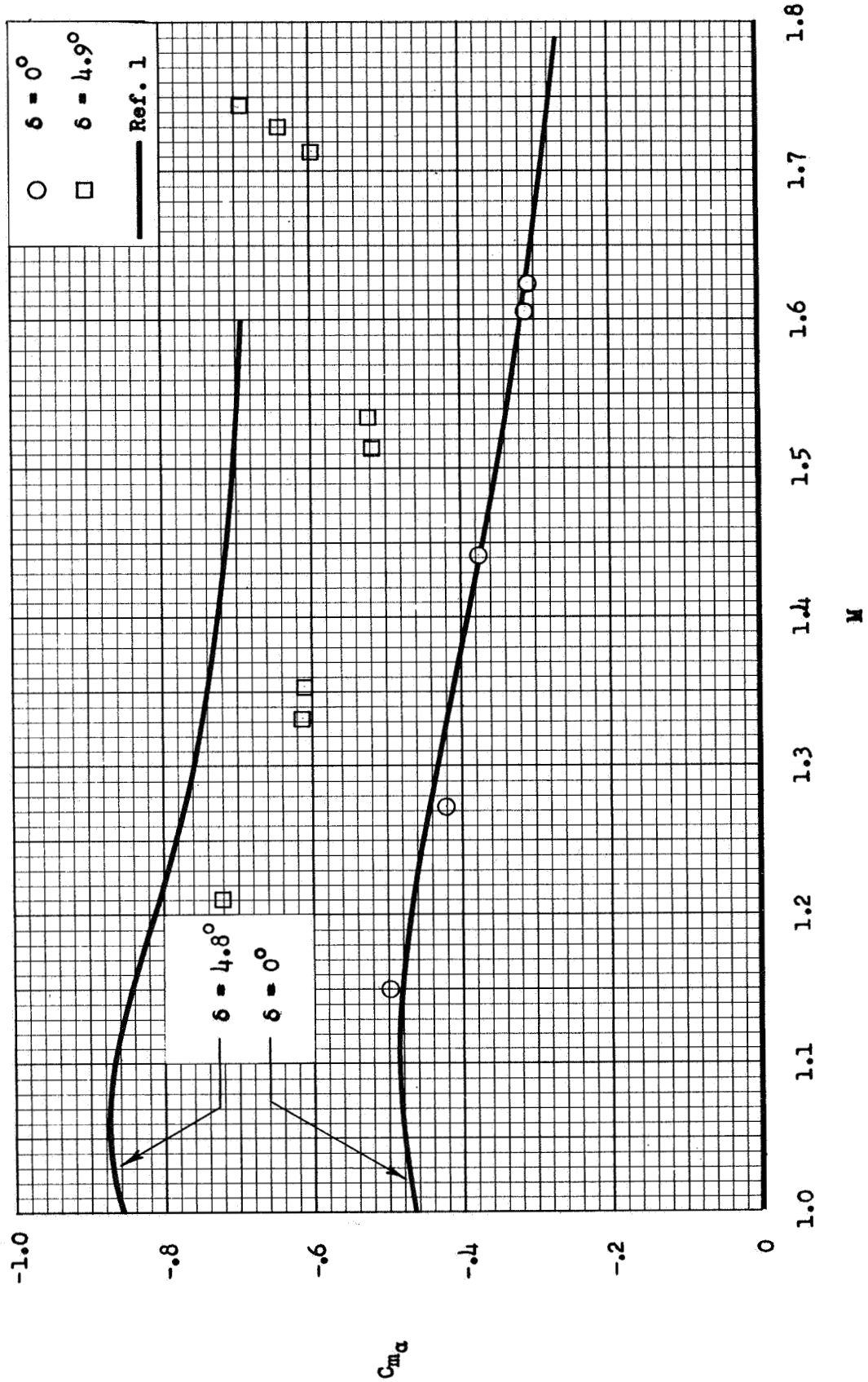


Figure 10.- Variation of static pitching-moment derivative with Mach number.

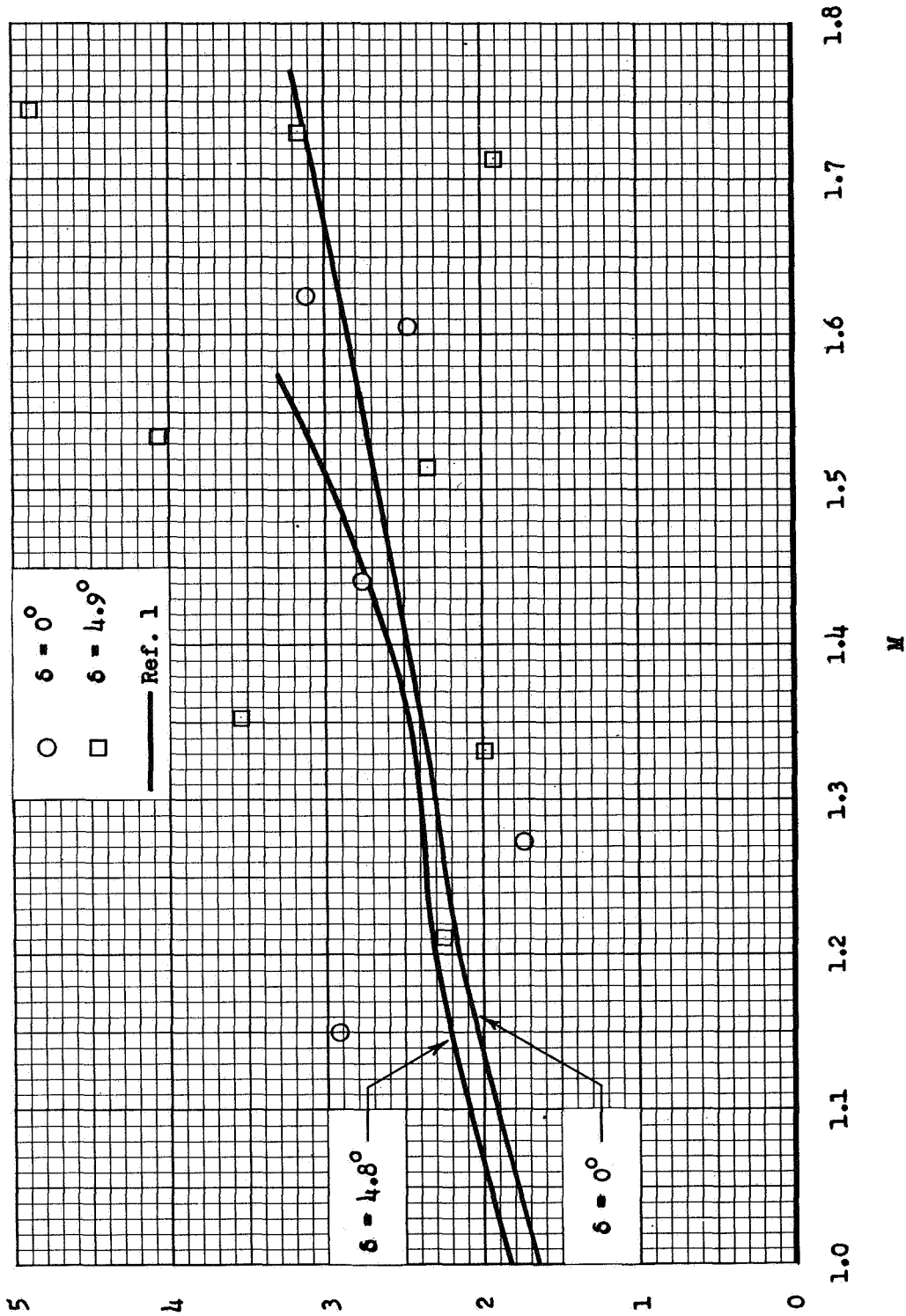


Figure 11.- Variation of exponential damping constant with Mach number.

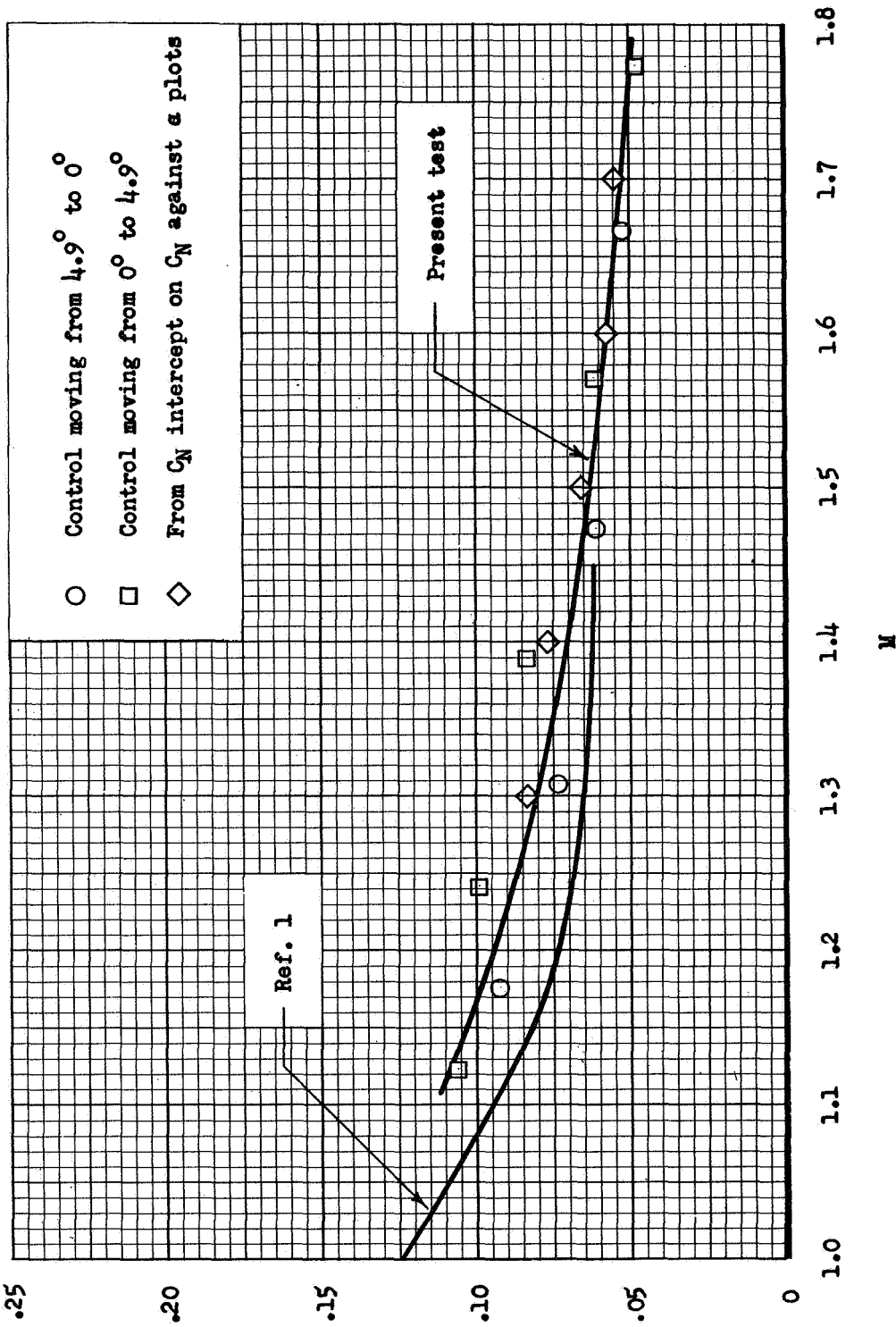


Figure 12.- Variation of normal force per unit control deflection with Mach number.

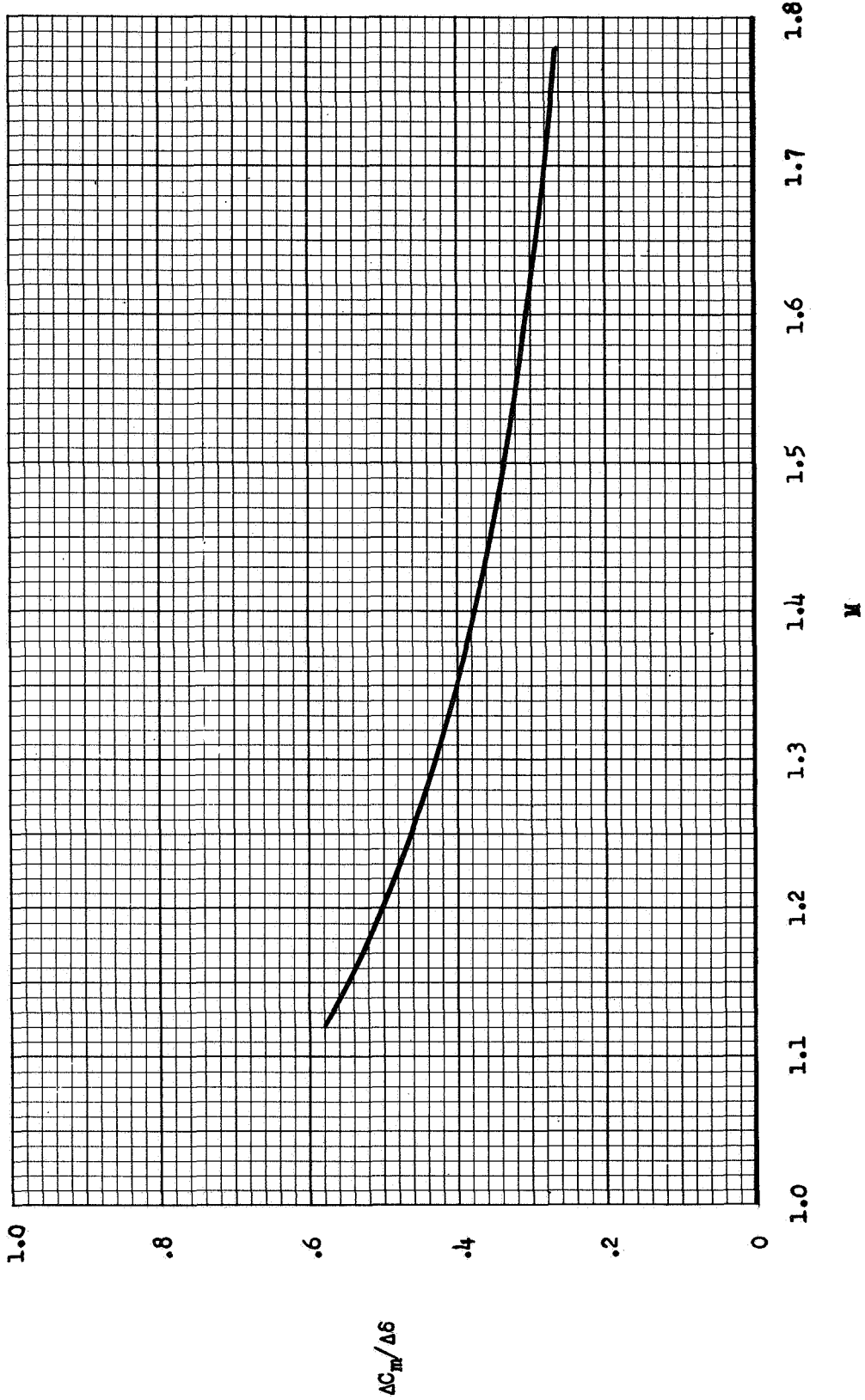


Figure 13.- Variation of control-surface pitching effectiveness with Mach number.

